A New Four Quadrants Drive Chopper for Separately Excited DC Motor in Low Cost Electric Vehicle

S. Arof, N. H. N. Diyanah, N. M. Noor, J. A. Jalil, P. A. Mawby and H. Arof

Abstract Four quadrants DC chopper systems are widely used in dc drive traction for electric vehicles. However, detail information on the design and method of operation for the systems were rarely addressed in the research literature. Accordingly, this study aimed to contribute on a new topology of a Four Quadrants Drive DC Chopper for separately excited dc motor. The chopper is designed to operate in five operation modes; driving, field weakening, generation, regenerative braking and resistive braking for the application of a low cost Electric Vehicle. The chopper modes of operation are further described and simulated using MATLAB/SIMULINK. Results on chopper performance, i.e. switching power losses, ripple torque and current, voltage drop and output power, regenerative braking power and control were discussed. The proposed chopper operations have been verified through experimental setup and the chopper is observed to be capable of performing the expected operations.

Keywords DC drive · Separtely excited machine · FQDC · DC chopper

S. Arof (✉) · N. H. N. Diyanah · N. M. Noor · J. A. Jalil
Electrical Electronic Automation Section, Universiti Kuala Lumpur, Malaysian Spanish Institute, Kulim Hi-Tech Park, 09000 Kulim, Kedah, Malaysia
e-mail: saharul@unikl.edu.my

N. H. N. Diyanah
e-mail: diyanahhisham94@gmail.com

N. M. Noor
e-mail: noramlee@unikl.edu.my

J. A. Jalil
e-mail: Julaida@unikl.edu.my

S. Arof · P. A. Mawby
University of Warwick School of Engineering, Coventry CV47AL, UK
e-mail: p.a.mawby@warwick.ac.uk

H. Arof
Engineering Department, Universiti Malaya, Jalan Universiti, 50603 Kuala Lumpur, Malaysia
e-mail: ahamzah@um.edu.my

© Springer Nature Switzerland AG 2019

M. H. Abu Bakar et al. (eds.), *Progress in Engineering Technology*,
Advanced Structured Materials 119, https://doi.org/10.1007/978-3-030-28505-0_10

1 Introduction

The emission of hydrocarbons not only pollutes the environment but also contributes to global warming, which melts the iceberg and increases the sea level. Using efficient Electric Vehicles (EV) and Hybrid Electric Vehicles (HEV) for transportation is one of the solutions to reducing global hydrocarbon emission. Unfortunately, the price of EV and HEV is expensive, making it unattainable for many people, especially those living in poor countries. Thus, there is a need for an efficient, compact drive system for EV and HEV that can reduce their cost and thus making them economical and affordable left [1–8] as an alternative.

It is well known that separately excited DC motors are easier to control and more stable in any mode of operation than series and shunt DC motors. To date, separately excited DC motors have been used in many prototypes or products for EV and HEV such as in the Peugeot 106, Citroen Saxo, GM EV and Lada [9, 10]. Research also has shown that separately-excited dc motor offers EV with longer distance traversed for a lower price [9] as depicted in Table 1. However, the last generation dc motors had disadvantages in their size, weight, performance and reliability. The separately excited DC motors can provide sufficient high starting torque and constant torque during operation. In the working region above base speed/nominal speed, DC motors still have higher torque compared to that of AC motors [11–14]. The motor can supply almost constant torque during their operation which is good for climbing a steep hill so that speed will not drop drastically. The motors also feature high electrical braking power due to less power loss [15, 16] and a very good speed and controllability for regenerative power. The regenerative power can be used to charge batteries or ultra-capacitors [17]. With the latest technology, DC motor manufacturers have developed better DC motors more

Table 1 Production of electric cars [2]

Manufacturer	Renault	Peugeot	Nissan
Model Name	Clio electric	106 electric	Hypermini
Driving type	Ac iduction	Separately excited	PM synch
Battery type	NiCd	NiCd	Li-ion
Max power O/P (kWh)	22	20	24
Voltage (V)	11.4	120	288
Battery energy capacity (kWh)	11.4	12	–
Top speed (km/h)	95	90	100
Claimed max range (km)	80	150	115
Charge time (h)	7	7–8	4
Price	$27,400	$27,000	$36,000

appropriate for EV/HEV applications. Such motors are equipped with higher power output, higher efficiency, smaller size, lighter weight, longer lasting carbon brush and commutator, lower operating voltage (less than 15 V) and easier to maintain structure (using modular concept construction) [10, 11]. The advanced brush technology for DC motors allows the motor to be used at low voltages [<50 V (35 V, 4500 A, 55 kW)] [11, 12] which results in lower power loss that guarantees longer travel distance.

In this paper, a novel four quadrants drive DC Chopper (FQDC) design shown in Fig. 1 is proposed to work with a separately excited DC motor. The system has resistive braking mode to achieve higher efficiency during braking. While the common H-bridge [15–17] shown in Fig. 2 utilizes at least two semiconductors at a time, the proposed FQDC uses only one semiconductor with the same operation. The proposed chopper design helps to improve power as well as to reduce ripple.

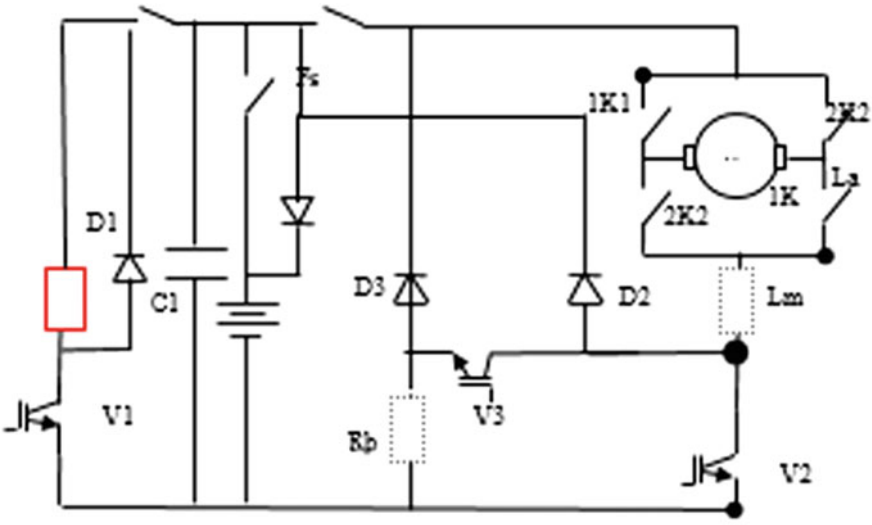

Fig. 1 Proposed FQDC topology

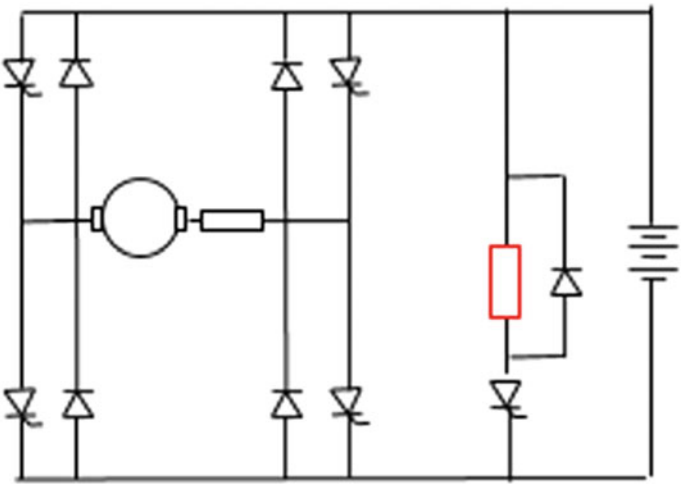

Fig. 2 Common H-bridge topology

2 Methodology

2.1 Four Quadrants Drive DC Chopper Operation Modes

The proposed FQDC is designed to work in five modes of operation; driving, field weakening, generator, regenerative braking and resistive braking. These modes of operation can be controlled by an AI controller such as expert system, fuzzy logic, self tuning fuzzy [2–4, 8], neural network as well as ANFIS. However, this paper focused only on the circuit operation of each modes of the proposed topology. Equations (1)–(4) are applicable for all chopper operation modes which represent the voltage, torque and current for the chopper. In those equations, B_{emf} is the back emf of the motor, K_b is the back emf constant and K_t is the torque motor constant. R_a and R_f are the motor coil resistances, ω is the angular speed and T_d is the motor torque. L_a is the armature inductance of the motor and L_m is an additional inductance connected in series with the armature windings to smoothen the motor armature current. V_t is the terminal voltage, L_f is the inductance of the field winding and R_b is the brake series resistor.

$$I_a = \frac{V_{batt} - I_a(R_a) - B_{emf}}{L_a} \tag{1}$$

$$I_f = \frac{V_{batt} - I_a(+R_f)}{L_f} \tag{2}$$

$$B_{emf} = K_v I_f \omega \tag{3}$$

$$T_d = K_t I_f I_a = \mathrm{J}\frac{d\omega}{dt} + B_w + T_L \tag{4}$$

2.2 Driving Mode

The successes of driving mode rely on the capacitor and the charge that is stored. Field and armature coil of separately excited motor has different resistance values where the field has almost a ten times or higher resistance value than the armature winding. During starting up, the back emf is zero without back emf to limit the armature current; the current would be high at the armature. Unlike power supply at home, an EC Battery has only certain limited current that it could provide. Due to big difference of armature and field winding the current from the battery is most likely preferred to flow to the armature coil living very small amount entering the field winding. So the lack of current will be topped by the capacitor current. This action is only required at the start of the motor rotation because once it has already started the motor from the armature current will decrease as a result of BEMF. In this case the current from battery is sufficient to be segregated to the armature and field winding. After releasing the pulses, the armature/load current that is governed by the preset control factor α (for the field igbt) and β (for the armature igbt) flows through the chopper. The switching of main IGBT *V1* and IGBT *V2* are determined by the control factor of α and β related to the duty ratio. The current path for driving operation is shown in Fig. 3.

In driving mode, the control factor α is set to unity and the control factor β is varied. This is an armature control mode. IGBT *V2* current will rise when the IGBT

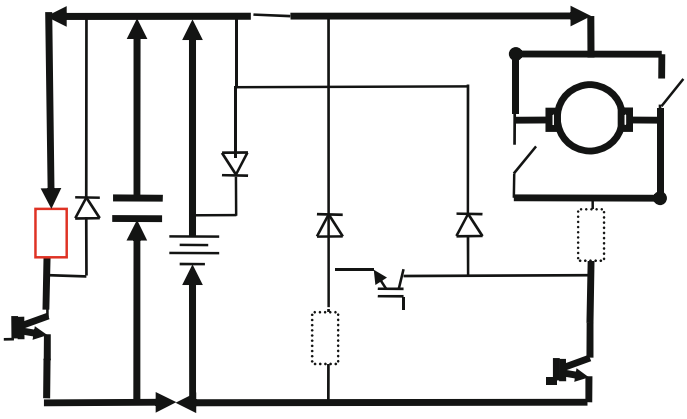

Fig. 3 FQDC in driving mode

V2 gate is fired on. The current rises gradually as its rate is limited by the circuit inductance. The values of armature and field currents when IGBT *V1* and *V2* are fired as in driving and field weakening mode can be described by Eqs. (5) and (6).

$$\left[-\left(\frac{R_f}{L_f}\right)\right][I_f]\left[\frac{1}{(L_f)}\right][V_{dc}K_{v1}] \tag{5}$$

$$\left[\frac{-R_a}{L_a}\right][I_a]\left[\frac{1}{L_a}-\frac{1}{L_a}\right]\begin{bmatrix} V_{dc}K_{v2} \\ B_{emf} \end{bmatrix} \tag{6}$$

2.3 Field Weakening Mode

When the field weakening is needed, the control factor β of IGBT *V2* is set to almost unity. The control factor α of IGBT *V1* is gradually decreased. This is the field control mode and the current path is shown in Fig. 4.

Reducing the current distribution at field winding decreases the back emf voltage as described by Eq. (1). The value of the current in the field coil is indirectly proportional to the value of α. Meanwhile, the armature current I_a rises as the IGBT *V1* duty ratio is decreased in proportion with the reduction in field current. The motor speed will increase due to the inflow of the armature current. This leads to an increase in the motor torque and speed. The mathematical equations used in the driving mode are also applicable to the field weakening mode. Only the control strategy differs between the two modes of operation.

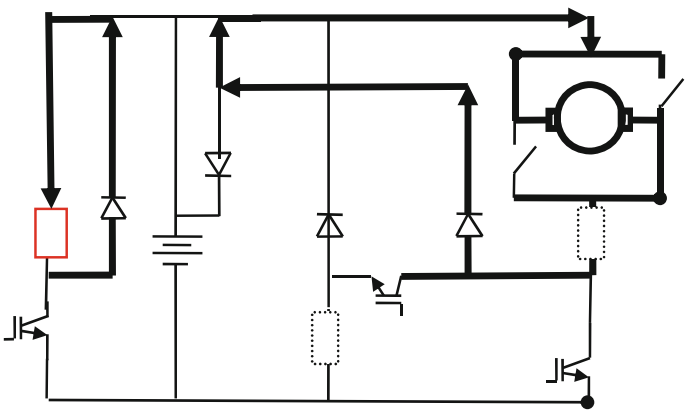

Fig. 4 FQDC in field weakening mode

2.4 Generator Mode

The kinetic energy that is available when the vehicle is going downhill can be used to generate electrical power to charge the batteries. The generated power is collected through the armature winding. The current has to flow through the field winding to establish the magnetic field. The IGBT *V1* is fired on to generate the voltage and current at the armature winding. The flow of current in the field and armature winding is shown in Fig. 5.

When contactor *2K2* is energized the armature current becomes negative due to the change in current direction. The generator mode reduces the motor speed since a counter torque motion is generated. In the generator mode, the field current and armature current are given by Eqs. (7) and (8).

$$\left[-\left(\frac{R_f}{L_f}\right)\right][I_f]\left[\frac{1}{(L_f)}\right][V_{dc}K_{v1}] \tag{7}$$

$$\left[\frac{-(R_{bh}+R_{batt}+R_a)}{L_a}\right][I_a]\left[\frac{1}{L_a}\right][B_{emf}] \tag{8}$$

2.5 Regenerative Braking Mode

The braking operation starts with the firing of IGBT *V1* until a minimum motor current is reached. As soon as IGBT *V1* is fired, current flows from the battery via IGBT *V1*. This guarantees a quick build-up of the motor voltage and currents via

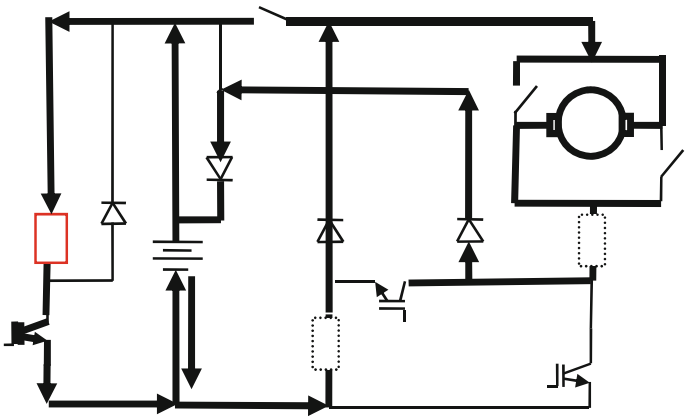

Fig. 5 FQDC in generator mode

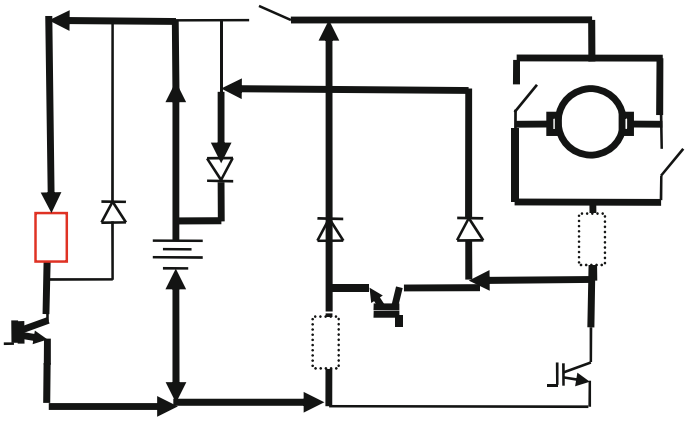

Fig. 6 FQDC in regenerative braking mode

armature terminal. The path of both excitation and load currents in this mode of operation is shown in Fig. 6.

Every time IGBT *V3* is triggered, it creates a short circuit path for the armature current to flow. Instead of going to the batteries to generate voltage, the current goes back to the armature coil which is short circuited. Due to the short circuit, a high current is induced. This high current creates a counter torque action against the motion of the motor which leads to braking or slowing down of the motor speed. The braking action reduces the kinetic energy of the vehicle and consequently the rotational speed of the motor. The armature and field current during regenerative braking can be represented by Eqs. (9) and (10).

$$\left[\frac{-(R_f)}{L_f}\right][I_f]\left[\frac{1}{L_f}\right]\left[V_{dc}K_{v1}/\frac{B_{emf}}{(1-K_{v3})}\right] \tag{9}$$

$$\left[\frac{-(R_a+R_{batt})}{(L_a)}/\frac{-(R_a+R_f)}{(L_a+L_f)}\right][I_a]\left[\frac{1}{(L_a)}\right]\left[\frac{B_{emf}}{(1-K_{v3})}\right] \tag{10}$$

2.6 Resistive Braking

The IGBT *V1* is fired to build up the needed generated voltage. These actions are illustrated as in Fig. 7.

The resistive braking mode starts when IGBT *V2* is fired. The duty ratio of IGBT *V2*, namely β, is varied according to the speed of the motor. IGBT *V1* is fired to keep the motor current constant. The generated voltage reduces proportionally with the decreasing vehicle speed. The firing of IGBT *V2* guarantees the motor current to commutate into the braking resistor R_b. The flow of the current can be regulated by

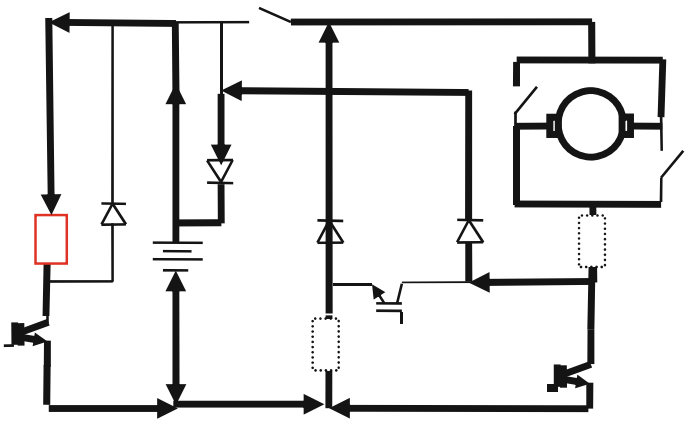

Fig. 7 FQDC in resistive braking mode

controlling the duty ratio of IGBT *V2*. The armature and field current during resistive braking can be represented by Eqs. (11) and (12) respectively.

$$\left[\frac{-(R_f)}{L_f}\right][I_f]\left[\frac{1}{L_f}\right]\left[V_{dc}K_{drv}/\frac{B_{emf}}{(1-K_{v3})}\right] \tag{11}$$

$$\left[\frac{-(R_a+R_{bh}+R_{batt})}{(L_a)}/\frac{-(R_a+R_{bh}+R_f)}{(L_a+L_f)}/\frac{-(R_a+R_{bh})}{(L_a)}\right][I_a]\left[\frac{1}{(L_a)}\right]\left[\frac{B_{emf}}{(1-K_{rgb})}/B_{emf}K_{v2}\right] \tag{12}$$

This type of braking mode can work independently or in combination with regenerative braking as shown in Fig. 8.

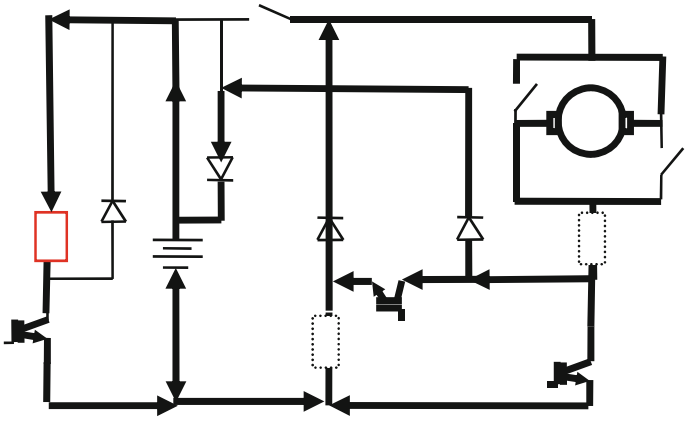

Fig. 8 Regenerative and resistive braking mode

If it works in combination the produce braking torque would be higher than the regenerative braking suitable for emergency brake. To work in combination the braking resistor value is set close to the regenerative braking short circuit resistance. The braking power of standalone resistive braking mode is much related to the value of braking resistor. The higher the braking resistor the lower the current flow through the braking resistor and the lower the braking torque produced.

2.7 Experimental Setup

In order to test the FQDC in all modes, an experimental set-up as shown in Figs. 9 and 10 were prepared. A 650 W separately excited dc motor shaft is coupled with another motor with inertia load (flywheel). Experimental results were captured using a data acquisition software. The experimental values of motor speed, armature current and field current were transferred to FQDC model in MATLAB/SIMULINK to validate the simulation model.

2.8 Results and Discussion

The Experimental and simulation results of the motor speed, armature current and field current for each modes of operation were shown in Figs. 11, 12, 13, 14 and 15. At the beginning of the driving mode, motor speed increases until it reaches the saturation level as shown in Fig. 11. Then the field weakening mode shown in Fig. 12 was initiated causing the motor speed to increase due to the rise in torque. In this mode, the armature current increases while the field current decreases.

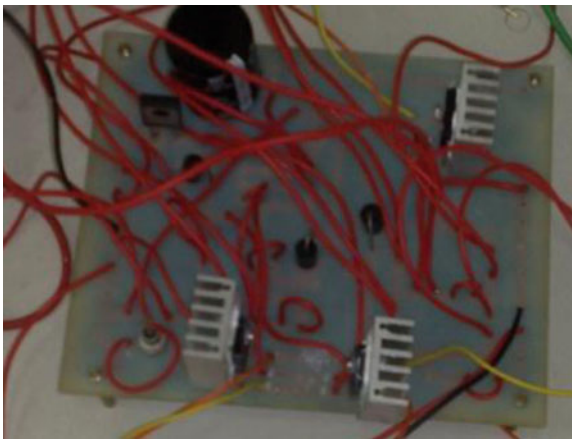

Fig. 9 FQDC for separately excited motor

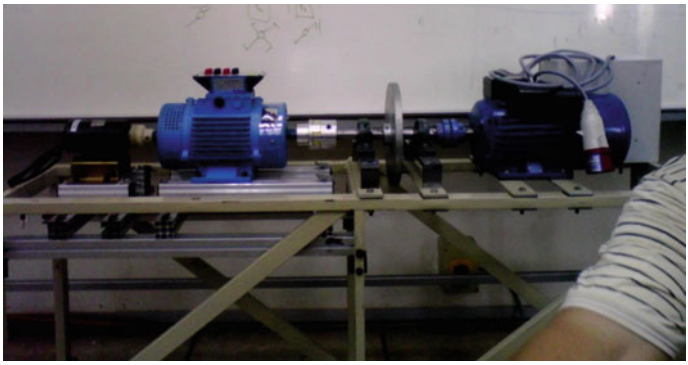

Fig. 10 Experimental set-up for the FQDC

Fig. 11 Driving mode

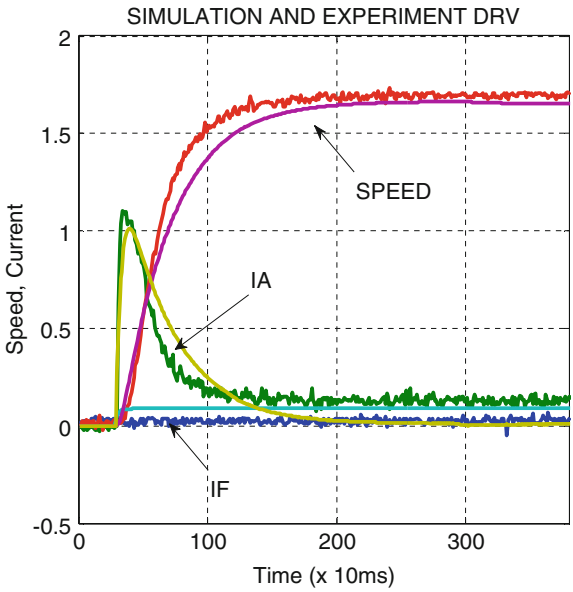

In the generator mode shown in Fig. 13, the field winding was charged with voltage to establish the magnetic field so that the armature coil could produce the generated voltage. In the graph the generated voltage shown has been normalized. During regenerative braking shown in Fig. 14, IGBT *V3* is turned on causing a short circuit path at the armature. The armature current rose in the opposite direction resulting in the developed torque to oppose the motor motion.

This caused the braking action. In the resistive braking mode shown in Fig. 15 the generated voltage was dissipated through the braking resistor. It is thus observed that the proposed chopper design behaved like a buck converter in all

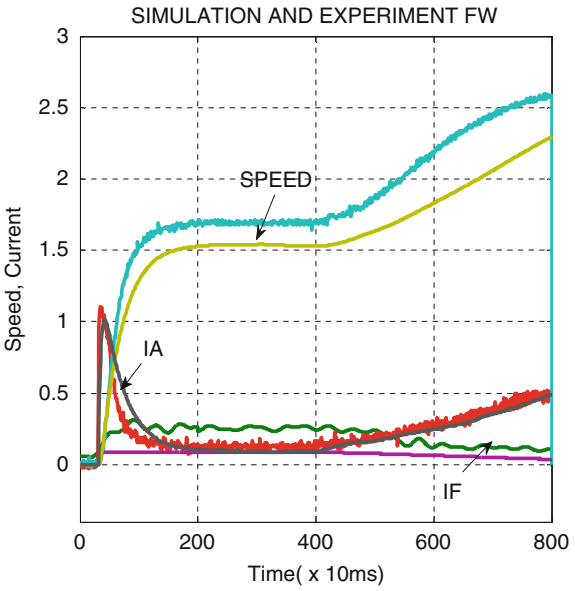

Fig. 12 Field weakening mode

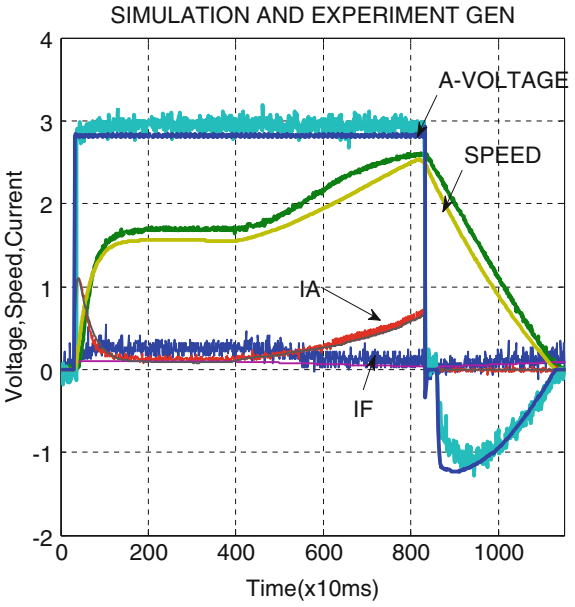

Fig. 13 Generator mode

operation modes except for regenerative braking. In regenerative braking mode, the chopper was observed to behave like a buck-boost converter.

The proposed FQDC offers several favorable performances such as lower power switching losses, smoother torque and current ripple, less voltage drop and higher

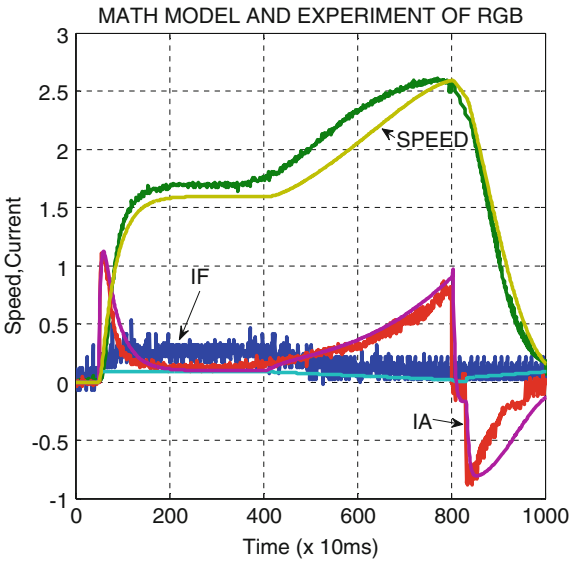

Fig. 14 Regenerative braking mode

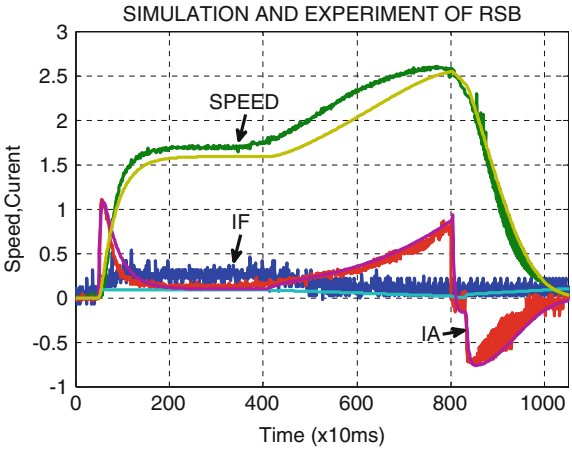

Fig. 15 Resistive braking mode

output power, as well as better braking performance as compared to the conventional H-bridge chopper. Every switching power electronics contributes to power switching losses. Losses during switch off are far greater than during switch on. The proposed chopper has single IGBT and single diode switching on and off during its operation. Meanwhile, the H-bridge has two power semiconductors and two diodes switching on and off during its operation. Thus, the switching power losses in H-bridge would be doubled. Figures 16, 17, 18 and 19 show the turn on and turns off power losses in IGBT and diodes respectively.

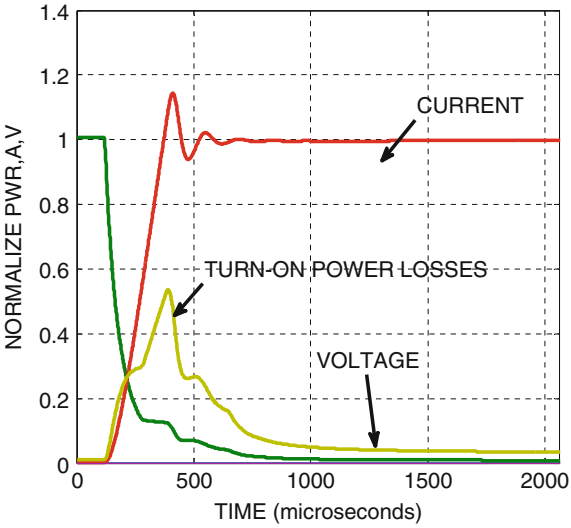

Fig. 16 IGBT turn on power losses

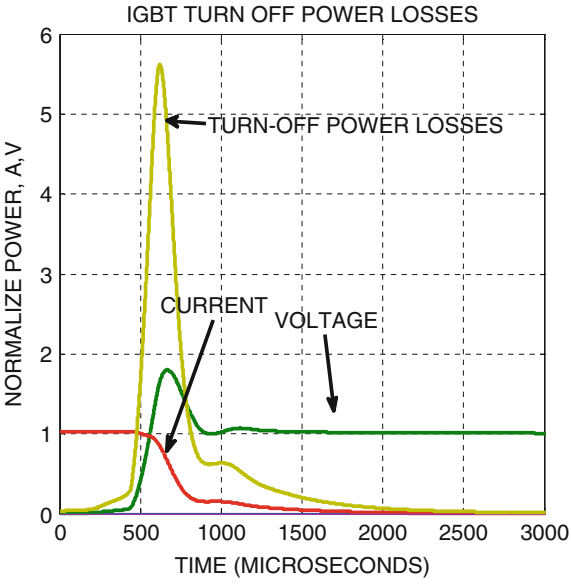

Fig. 17 IGBT turn off power losses

The proposed chopper also offers smoother armature current and torque shown in Figs. 20 and 21, as compared to H-bridge due to a single IGBT firing. It is difficult to get the IGBT in H-Bridge fires at the same time. The proposed chopper used contactor so that the voltage stored in inductor winding will be easily discharged.

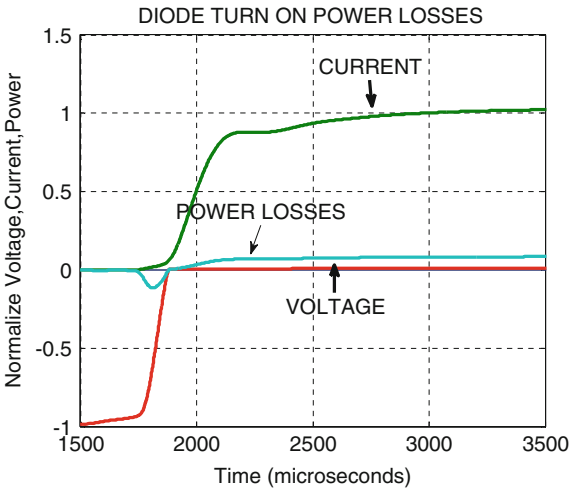

Fig. 18 Diode turn on power losses

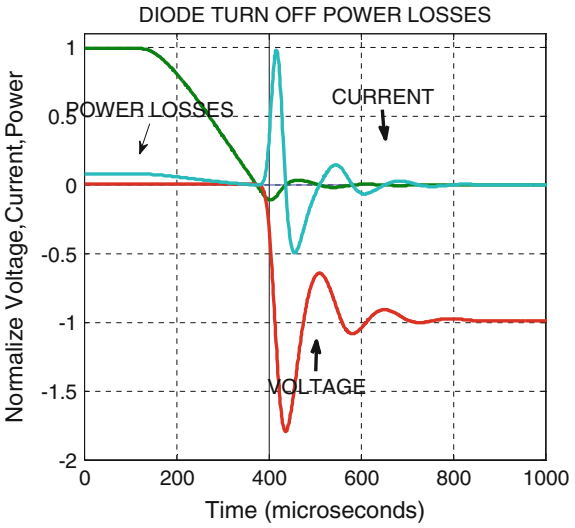

Fig. 19 Diode turn off power losses

Accordingly, voltage at the inductor winding during IGBT turn off can easily be removed in this chopper circuit as compared to voltage in the H-bridge. Voltage stored in H-bridge has to be returned to the battery. When the stored voltage is lower than the battery voltage, the clamping diode will switch off thus blocked the stored voltage avoiding it to return to its origin. When the IGBT is switch on again, the residual voltage stored in the circuit causes ripple in armature current. The influence of low ripple has current results in low ripple torque.

Every semiconductor has voltage drop during turn on. This is called the voltage collector emitter saturation. While the proposed chopper running on single IGBT,

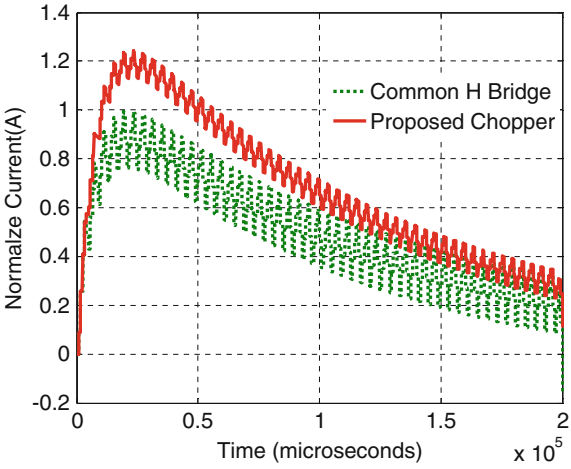

Fig. 20 Ripple current

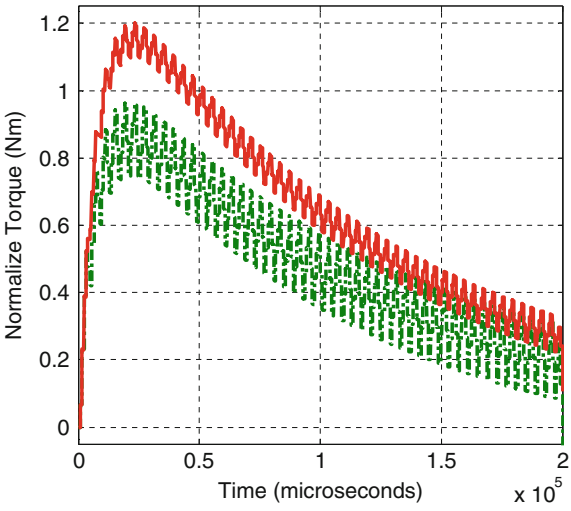

Fig. 21 Ripple torque

H-bridge is running on two IGBT resulted in a double voltage drop. Since the chopper has less voltage drop as compared to the one in H-bridge, therefore its armature current is observed to be higher than in H-bridge. As higher current produces more torque and higher speed, thus the chopper output power is observed to be higher. The current and output power is depicted in Figs. 22 and 23 respectively.

As the battery state of charge is almost 100%, the voltage difference between the charging voltage and battery terminal voltage is getting lower and resulting in a lower charging current. However, braking is required at this moment. Since the battery current is low, thus armature current is also low. Accordingly the braking torque produced is also low. In order to achieve the required braking torque, IGBT *V3* is fired. The IGBT *V3* caused a rise in armature current due to the effect of

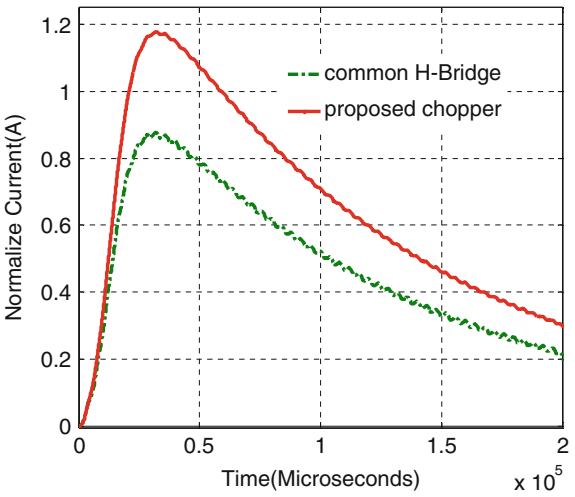

Fig. 22 Armature current

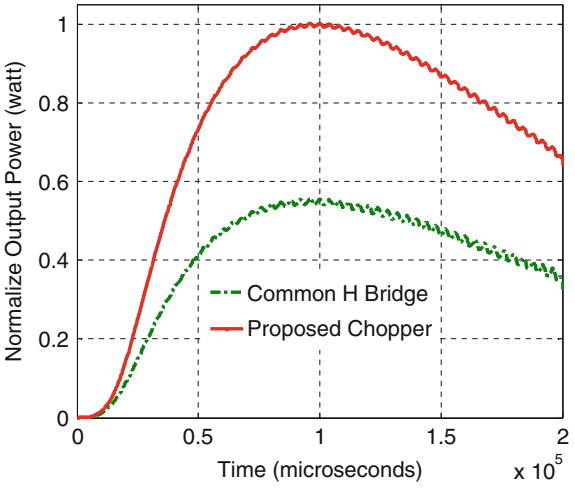

Fig. 23 Braking effect at high SOC

armature voltage short circuited. Consequently, the braking torque is increased as shown in Fig. 24. In the case of higher braking torque is needed, i.e. an emergency brake, IGBT *V3* can be further controlled to produce higher braking torque as shown in Fig. 25 thus the EV speed will decelerate faster. Since the braking torque is influenced by both field and armature currents, therefore any changes in vehicle speed will affect the field current. Subsequent change in vehicle speed leads to change in braking torque. Since the braking torque produced is always nonlinear, thus a proper control of IGBT *V3* provides better control in the braking torque, resulting in linear braking effect as shown in Fig. 25.

Resistive braking mode offers another type of electrical braking. In the case of a higher braking action is required, a lower braking value of braking resistor is

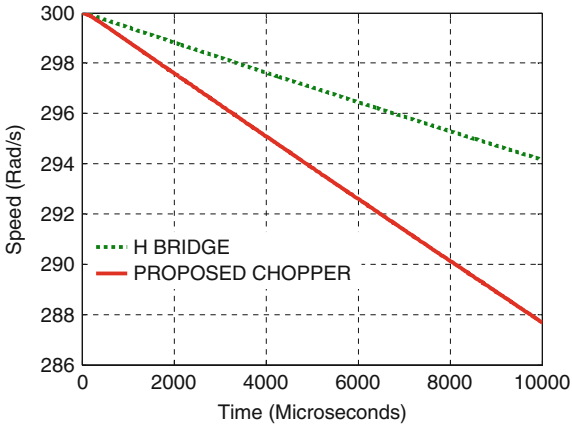

Fig. 24 Higher braking effect in regenerative braking

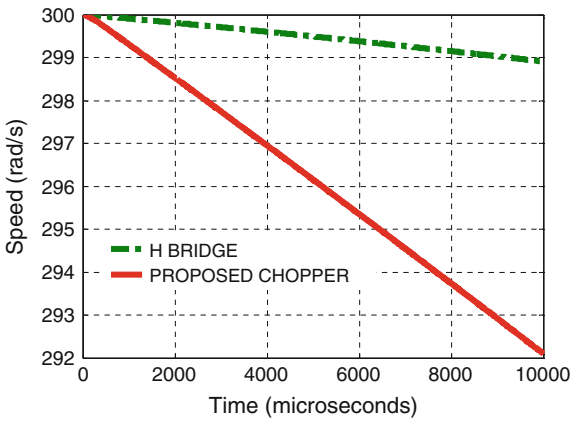

Fig. 25 Linear braking efect in regenerative braking

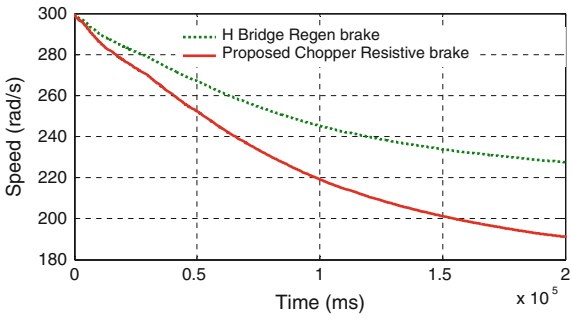

Fig. 26 Resistive braking effect

chosen. As lower braking resistor causes a rise in armature current, hence higher braking torque can be generated resulting a drop in motor speed as shown in Fig. 26. Resistive braking mode is able to extend the electrical braking before mechanical brake takes over.

3 Conclusions

The proposed four quadrants drive DC chopper design has been simulated and experimented to drive a separately excited DC motor for five modes of operation. The experimental results revealed that chopper is capable to operate in all the five modes. However, the FQDC performances such as lower power switching losses, smoother torque and current ripple, less voltage drop and higher output power, as well as better braking performance as compared to the conventional H-bridge chopper were simulated using Matlab/Simulink mathematical model. In summary, the FQDC has great potential to be utilized in EV application due to simple and excellence controllability thus made it suitable for applications in this cost effective EV solution.

References

1. Arof, S., Jalil, J.A., Yaakop, N.M., Mawby, P.A., Arof, H.: Series motor four quadrants drive DC chopper. Part 1: overall. In: IEEE International Conference on Power Electronics (2014). https://doi.org/10.1109/pecon.2014.7062468
2. Arof, S., Khairulzaman, M., Jalil, A.K., Arof, H., Mawby, P.A.: Self tuning fuzzy logic controlling chopper operation of four quadrants drive DC chopper for low cost electric vehicle. In: 6th International Conference on Intelligent Systems, Modeling and Simulation, pp 24–40. IEEE Computer Society (2015). https://doi.org/10.1109/isms.2015.34
3. Arof, S., Khairulzaman, M., Jalil, A.K., Arof, H., Mawby, P.A.: Artificial intelligence controlling Chopper operation of four quadrants drive DC Chopper for low cost electric vehicle. Int. J. Simul. Sci. Technol. (2015). https://doi.org/10.5013/ijssst.a.16.04.03,2015.ijsst
4. Arof, S., Jalil, J.A., Kamaruddin, N.H., Yaakop, N.M., Mawby, P.A., Arof, H.: Series motor four quadrants drive DC chopper. Part 2: driving and reverse with direct current control. In: International Conference on Power Electronics, pp. 775–780 (2016). ISBN 978-1-5090-2547-3/16. https://doi.org/10.1109/pecon 2016.7951663
5. Arof, S., Hassan, H., Rosyidi, M., Mawby, P.A., Arof, H.: Implementation of Series motor four quadrants drive DC chopper for DC drive electric car and LRT. J. Appl. Environ. Biol. Sci. J. Appl. Environ. Biol. Sci. **7**(3S), 73–82 (2017)
6. Arof, S., Noor,N.M, Elias, F., Mawby, P.A., Arof, H.: Investigation of chopper operation of series motor four quadrants DC chopper. J. Appl. Environ. Biol. Sci. J. Appl. Environ. Biol. Sci. **7**(3S), 49–56 (2017)
7. Arof, S., Diyanah, N.H., Mawby, P.A., Arof, H.: Study on implementation of neural network controlling four quadrants direct current chopper: part 1: using single neural network controller with binary data output. In: Advanced Engineering for Processes and Technologies, pp. 37–57 (2019)
8. Processor in the loop for testing series motor four quadrants drive direct current chopper for series motor driven electric car: part 1: chopper operation modes testing. In: Advanced Engineering for Processes and Technologies, pp. 59–76 (2019). https://doi.org/10.1007/978-3-030-05621-6_5
9. Westbrook, M.H.: The Electric and Hybrid Electric Vehicle. SAE (2001)
10. Husain, I.: Electric and Hybrid Electric Vehicles, Design Fundamentals. CRC Press, Boca Raton
11. Oak Ridge National Laboratory: Advanced Brush Technology for DC Motors (2009). http://peemrc.ornl.gov/projects/emdc3.jpg

12. Oak Ridge National Laboratory: Soft-commutated direct current (dc) motor (2009). Available: www.ornl.gov/etd/peemrc
13. Heinrich, Walter Rentsch, Herbert Dr.-Ing., ABB Industry: guide to variable speed drives. Technical Guide No. 41180 D-68619 LAMPERTHEIM, Germany, 3ADW 000 059 R0201 REV B (02.01), DCS 400/DCS 500/DCS 600: ABB (2003)
14. Bansal, R.C.: . Electric vehicle. In: Handbook of Automotive Power Electronics and Motor Drives. Taylor & Francise Group, CRC Press, Boca Raton
15. Rashid, M.H.: Power Electronics, Circuits, Devices and Applications, 3rd ed. Prentice Hall, Upper Saddle River
16. Senthil Kumar, N., Sasasivam, V., Muruganandam, M.: A low cost four-quadrant chopper—fed embedded DC drive using fuzzy controller. J. Electr. Power Comp. Syst. **35**, 907–920
17. Joshi, D., Bansal, R.C.: Performance evaluation of multiquadrant DC drive using fuzzy-genetic approach. J. Electr. Syst. (JES) **5**(4) (2009)